Int. J. Solids Structures Vol. 22, No. 1, pp. 73–86, 1986
Printed in Great Britain.

0020–7683/86 $3.00 + .00

STEADY-STATE RING-LOAD PRESSURE ON A BORE HOLE SURFACE

R. PARNES†
Department of Solid Mechanics, Materials and Structures, Faculty of Engineering, Tel-Aviv University,
Ramat-Aviv 69978, Tel-Aviv, Israel

(*Received* 28 *April* 1984)

Abstract—The response of an elastic medium to a ring-load pressure on the surface of a cylindrical cavity, having a harmonic time dependency is studied. Integral representations of the stress and displacement fields are obtained, and numerical results along a radial line emanating from the point of load application are presented. The response is observed to occur due to *P*-, *S*- and surface waves whose radiation depends on a critical forcing frequency. The dynamic effect is represented finally by dynamic amplification factors, and the increased radial penetration of the response is analyzed in terms of the radiation of the excited waves.

1. INTRODUCTION

The application of tractions to the surface of a bore contained in an elastic medium has been the subject of investigation by several authors[1–6]. Analytic solutions for statically applied radial pressures acting over a finite segment of the bore were given in [1, 2]. More recently the static response of applied tractions, both pressure and torsional loads, applied as a ring load was determined, and numerical results presented[3].

The dynamic response of a medium to a suddenly applied bore pressure loading along the entire bore surface was given by Selberg[4]. Later, Jordan presented the solution to a similar dynamically applied pressure loading over a segment of the bore[5]. In addition, the problem of an infinite medium containing a cylindrical elastic shell undergoing dynamic axisymmetric deformations was considered in [6]. The steady-state response to a harmonically applied torsional line load was recently given by the author[7].

In the present investigation we consider the problem of the steady-state response of an elastic medium to a radial pressure ring load, having a harmonic time dependency and applied on the surface of the bore. The response is necessarily more complex than that of the preceding case, since both dilatational and equivoluminal effects enter into the solution.

Integral representations for the displacement and stress fields are obtained, and numerical results are given for the displacements and stress components along a radial line emanating from the point of load application. Physical interpretations of the results are presented, and the dynamic effect as measured by dynamic amplification factors is studied. These reveal that far greater radial penetration occurs in the dynamic case, as compared to the corresponding static case, which may be attributed to the radiation of outgoing *P*- and *S*-waves, as well as excited surface waves for certain ranges of applied frequency.

The present problem is of interest, for example, in the field of hydraulic and formation fracture; fields in which considerable empirical results are available[8, 9], but in which significant investigations are still required in order to obtain a more complete understanding of the phenomena. Although the model represents a first approximation to the actual *in situ* conditions, the results presented would appear to suggest that dynamic application of pressure loadings, causing greater radial penetration, could lead to larger regions of high stress level and, hence, larger zones of crack formation.

† Presently on leave. Current address: Laboratoire de Mécanique des Solides, Ecole Polytechnique, 91128 Palaiseau, France.

2. GENERAL FORMULATION

Consider a cylindrical bore of radius $r = a$ in a linear isotropic elastic medium referred to a fixed nondimensional coordinate system ($\rho = r/a$, θ, $\xi = z/a$) whose origin lies on the axis of the bore. A radial pressure, prescribed as a uniform line load along a circle at $z = 0$, is applied and acts harmonically in time with frequency $\omega = 2\pi f$ (Fig. 1). The stresses on the boundary $\rho = 1$ are then

$$\sigma_{rr} = \frac{P}{a}\,\delta(\xi)\,e^{-i\omega t}, \qquad \sigma_{rz} = 0, \qquad \sigma_{r\theta} = 0, \tag{1}$$

where $\delta(\xi)$ is the Dirac-delta function.

The axisymmetric displacements

$$\mathbf{u}(\rho, \xi, t) = w\mathbf{k}_r + u\mathbf{k}_z \tag{2}$$

must satisfy the equation of motion for the elastic medium

$$\mu\nabla^2\mathbf{u} + (\lambda + \mu)\nabla\nabla\cdot\mathbf{u} = a^2\rho_D\ddot{\mathbf{u}}, \tag{3}$$

where μ and λ are the Lamé constants, ρ_D is the mass density, and where

$$\nabla \equiv \frac{\partial}{\partial\rho}\mathbf{k}_r + \frac{1}{\rho}\frac{\partial}{\partial\theta}\mathbf{k}_\theta + \frac{\partial}{\partial\xi}\mathbf{k}_z. \tag{4}$$

Potential functions $\Phi(\rho, \xi, \tau)$ and $\Psi(\rho, \xi, \tau)$ are defined such that the displacement components are given, according to Helmholtz's theorem, by

$$w(\rho, \xi) = 1/a\left(\Phi_{,\rho} - \frac{1}{a}\Psi_{,\rho\xi}\right) \tag{5a}$$

$$u(\rho, \xi) = 1/a\left[\Phi_{,\xi} + \frac{1}{a}\left(\psi_{,\rho\rho} + \frac{1}{a\rho}\psi_{,\rho}\right)\right] \tag{5b}$$

(Derivatives are denoted by commas and subscripts, e.g. $\Psi_{,r} \equiv \partial\Psi/\partial r$, etc.) These potential functions, valid for axisymmetric displacements, are a particular case of the more general functions used by the author in [10].

Substituting eqns (5) in eqn (3), the potential functions must satisfy the wave equations

$$\nabla^2\Phi = \frac{1}{R_c^2}\frac{\partial^2\Phi}{\partial\tau^2}, \tag{6a}$$

$$\nabla^2\psi = \frac{\partial^2\psi}{\partial\tau^2}, \tag{6b}$$

where

$$\tau = C_s\,t/a \tag{6c}$$

represents the nondimensional time, and where

$$R_c \equiv C_p/C_s = \left[\frac{2(1-\nu)}{1-2\nu}\right]^{1/2} \tag{7}$$

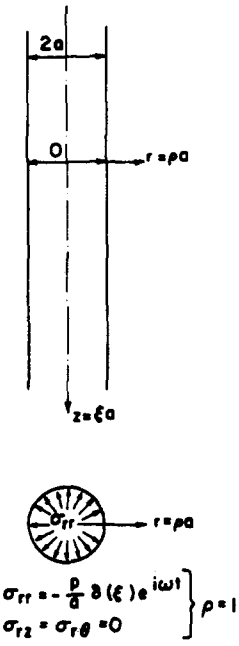

Fig. 1. Geometry of problem.

represents the ratio of the propagation speeds, C_p and C_s of P- and S-waves, respectively, in the medium.

Substituting eqns (5) in the elastic stress–strain relations, and using eqns (6), the stresses are readily expressed in terms of the potential function. Explicit expressions are given in [11].

The last boundary condition of eqn (1) is found to be satisfied identically, while the first two become

$$\frac{\lambda}{R_c^2}\Phi_{,\tau\tau} + 2\mu\left(\Phi_{,\rho\rho} - \frac{1}{a}\Psi_{,\rho\rho\xi}\right)\Big|_{\rho=1} = \mathrm{Pa}\,\delta(\xi)\,e^{-i\Omega\tau}, \tag{8a}$$

$$2\Phi_{,\rho\xi} + \frac{1}{a}(\Psi_{,\tau\tau\rho} - 2\Psi_{,\xi\xi\rho})\,|_{\rho=1} = 0, \tag{8b}$$

where

$$\Omega = \omega a/C_s \tag{9}$$

is the nondimensional frequency.

3. GENERAL SOLUTION

Using the integral representation for the Dirac-delta function[12],

$$\delta(\xi) = \frac{1}{\pi}\int_0^\infty \cos\alpha\xi\,d\alpha, \tag{10}$$

the boundary condition, eqn (8a), becomes

$$\left[\frac{\lambda}{R_c^2}\Phi_{,\tau\tau} + 2\mu\left(\Phi_{,\rho\rho} - \frac{1}{a}\Psi_{,\rho\rho\xi}\right)\right]\Big|_{\rho=1} = \frac{\mathrm{Pa}}{\pi}\int_0^\infty \cos\alpha\xi\,d\alpha\,e^{-i\Omega\tau}. \tag{11}$$

The general steady-state solutions for the potentials representing outgoing waves, and which are compatible with the boundary condition of eqn (11), are

$$\Phi(\rho, \xi, \tau) = \frac{1}{\pi}\int_0^\infty C(\alpha)\, H_0^{(1)}(\gamma_p\rho)\cos\alpha\xi\, d\alpha\, e^{-i\Omega\tau}, \tag{12a}$$

$$\Psi(\rho, \xi, \tau) = \frac{1}{\pi}\int_0^\infty D(\alpha)\, H_0^{(1)}(\gamma_s\rho)\sin\alpha\xi\, d\alpha\, e^{-i\Omega\tau}, \tag{12b}$$

where

$$\gamma_p = (\Omega^2/R_c^2 - \alpha^2)^{1/2}, \tag{13a}$$

$$\gamma_s = (\Omega^2 - \alpha^2)^{1/2}, \tag{13b}$$

and where $H_n^{(1)}$ is the Hankel function of the first kind of order n.

The arbitrary constants, $C(\alpha)$ and $D(\alpha)$, are obtained by satisfying the boundary conditions, eqns (8b) and (11) [For simplification the superscript (1) is dropped here and subsequently in writing the Hankel function, it being clearly understood that $H_n(x) \equiv H_n^{(1)}(x)$. Furthermore, for values at $\rho = 1$, the Hankel functions will be written here and below using the following simplified notation: $H_n \equiv H_n(\gamma_p)$, $\bar{H}_n \equiv H_n(\gamma_s)$.]

$$C = -\frac{[a(2\alpha^2 - \Omega^2)\bar{H}_1]}{2\mu\Lambda}P, \tag{14a}$$

$$D = -\frac{\alpha a^2\gamma_p H_1}{\mu\gamma_s\Lambda}P, \tag{14b}$$

where

$$\Lambda = -2\alpha^2\gamma_s\gamma_p\bar{H}_0H_1 + (2\alpha^2 - \Omega^2)\left(\frac{\lambda}{2\mu}\frac{\Omega^2}{R_c^2} + \gamma_p^2\right)H_0\bar{H}_1 + \Omega^2\gamma_pH_1\bar{H}_1. \tag{15}$$

Substitution of eqns (12) with the known constants in eqns (5) then yields the displacements, viz.

$$\frac{w\mu}{P} = \frac{1}{\pi}\int_0^\infty\frac{\gamma_p}{\Lambda}\left[\frac{1}{2}(2\alpha^2 - \Omega^2)\bar{H}_1H_1(\gamma_p\rho) - \alpha^2H_1H_1(\gamma_s\rho)\right]\cos\alpha\xi\, d\alpha\, e^{-i\Omega\tau}, \tag{16a}$$

$$\frac{u\mu}{P} = \frac{1}{\pi}\int_0^\infty\frac{\alpha}{\Lambda}\left[\frac{1}{2}(2\alpha^2 - \Omega^2)\bar{H}_1H_0(\gamma_p\rho) - \gamma_s\gamma_pH_1H_0(\gamma_s\rho)\right]\sin\alpha\xi\, d\alpha\, e^{-i\Omega T}. \tag{16b}$$

Similarly upon making the proper substitutions and algebraic manipulations the following expressions are obtained for the stresses[11]:

$$\frac{\sigma_{rr}a}{P} = \frac{1}{\pi}\int_0^\infty\frac{1}{\Lambda}\left[\left(\frac{\lambda\Omega^2}{2\mu R_c^2} + \gamma_p^2\right)(2\alpha^2 - \Omega^2)\bar{H}_1H_0(\gamma_p\rho) - \frac{\gamma_p}{\rho}(2\alpha^2 - \Omega^2)\bar{H}_1H_1(\gamma_p\rho)\right.$$
$$\left. + \frac{2\alpha^2\gamma_p}{\rho}H_1H_1(\gamma_s\rho) - 2\alpha^2\gamma_p\gamma_sH_1H_0(\gamma_s\rho)\right]\cos\alpha\xi\, d\alpha\, e^{-i\Omega\tau}, \tag{17a}$$

$$\frac{\sigma_{\theta\theta}a}{P} = \frac{1}{\pi}\int_0^\infty\frac{1}{\Lambda}\left[\frac{\lambda\Omega^2}{2\mu R_c^2}(2\alpha^2 - \Omega^2)\bar{H}_1H_0(\gamma_p\rho) + \frac{\gamma_p}{\rho}(2a^2 - \Omega^2)\bar{H}_1H_1(\gamma_p\rho)\right.$$
$$\left. - \frac{2\alpha^2\gamma_p}{\rho}H_1H_1(\gamma_s\rho)\right]\cos\alpha\xi\, d\alpha\, e^{-i\Omega\tau}, \tag{17b}$$

$$\frac{\sigma_{zz}a}{P} = \frac{1}{\pi}\int_0^\infty \frac{1}{\Lambda}\left[\frac{1}{2}\left(\frac{\lambda\Omega^2}{\mu R_c^2} + 2\alpha^2\right)(2\alpha^2 - \Omega^2)\bar{H}_1 H_0(\gamma_p\rho) + 2\alpha^2\gamma_s\gamma_p H_1 H_0(\gamma_s\rho)\right]\cos\alpha\xi\, d\alpha\, e^{-i\Omega\tau}, \tag{17c}$$

$$\frac{\sigma_{rz}a}{P} = \frac{1}{\pi}\int_0^\infty \frac{\alpha(2\alpha^2 - \Omega^2)}{\Lambda}\gamma_p[H_1H_1(\gamma_s\rho) - \bar{H}_1H_1(\gamma_p\rho)]\sin\alpha\xi\, d\alpha\, e^{-i\Omega\tau}. \tag{17d}$$

It is now observed that γ_p and γ_s, as defined by eqns (13), are either real or imaginary, depending on the value of the ratios $R_c^2\alpha^2/\Omega^2$ and α^2/Ω^2, with respect to unity. Thus we may distinguish three subranges: (a) $0 < \alpha < \Omega^2/R_c^2$; (b) $\Omega^2/R_c^2 < \alpha^2 < \Omega^2$; (c) $\Omega^2 < \alpha^2 < \infty$. (It is noted that from its definition, $R_c \geq \sqrt{2}$.) In the first range, both γ_s and γ_p are real; in the second, γ_s is real, while γ_p is imaginary; in the latter range, both γ_s and γ_p are imaginary. It therefore becomes particularly useful to subdivide the infinite range into the above three subranges; this will become especially essential in interpreting the subsequent results.

To this end, we note the relation[13]

$$K_n(x) = \frac{\pi}{2}e^{1/2(n+1)\pi i}H_n^{(1)}(ix), \tag{18}$$

where $K_n(x)$ is the modified Bessel function of order n.

We first define the nondimensional parameter

$$q = \alpha/\Omega \tag{19}$$

and let

$$\beta_p = \Omega b_p, \tag{20a}$$

$$\beta_s = \Omega b_s, \tag{20b}$$

where

$$b_p = \left|\frac{1}{3} - q^2\right|^{1/2}, \tag{21a}$$

$$b_s = |1 - q^2|^{1/2} \tag{21b}$$

Expressions for the displacements component u_i (w or u) and the stress components σ_{ij} are then written in the following form for $\nu = 0.25$. (For simplification, all subsequent expressions and results are given with $\nu = .25$. For this value $R_c = \sqrt{3}$.)

$$\frac{\mu u_i}{P} = \frac{\Omega}{\pi}\left(\int_0^{1/\sqrt{3}}\frac{\Gamma_{u_i}^{(a)}}{\Lambda^{(a)}}dq + \int_{1/\sqrt{3}}^1\frac{\Gamma_{u_i}^{(b)}}{\Lambda^{(b)}}dq + \int_1^\infty\frac{\Gamma_{u_i}^{(c)}}{\Lambda^{(c)}}dq\right)e^{-i\Omega\tau}, \tag{22a}$$

$$\frac{\sigma_{ij}a}{P} = \frac{\Omega}{\pi}\left(\int_0^{1/\sqrt{3}}\frac{\Gamma_{ij}^{(a)}}{\Lambda^{(a)}}dq + \int_{1/\sqrt{3}}^1\frac{\Gamma_{ij}^{(b)}}{\Lambda^{(b)}}dq + \int_1^\infty\frac{\Gamma_{ij}^{(c)}}{\Lambda^{(c)}}dq\right)e^{-i\Omega\tau}, \tag{22b}$$

where

$$\Lambda^{(k)} = -2\Omega q^2 b_s b_p G_{01}^{(k)}(\beta_s, \beta_p) - \frac{\Omega}{2}(2q^2 - 1)^2 F_{10}^{(k)}(\beta_s, \beta_p) + b_p F_{11}^{(k)}(\beta_s, \beta_p), \quad k = a, b, c, \tag{23}$$

and where $\Gamma_{ui}^{(k)}$ and $\Gamma_{ij}^{(k)}$ (k = a, b, c) are the numerators of the integrands for the various quantities expressed in terms of $F_{mn}^{(k)}$ and $G_{mn}^{(k)}$, which denote (in each region k = a, b, or c) the following combinations of Hankel and/or Bessel functions:

$$F_{mn}^{(a)}(x, y) = H_m(x)H_n(y), \qquad F_{mn}^{(b)}(x, y) = -H_m(x)K_n(y),$$
$$F_{mn}^{(c)}(x, y) = K_m(x)K_n(y), \qquad m = 0, 1; \quad n = 0, 1, \tag{24}$$

$$G_{mn}^{(a)}(x, y) = H_m(x)H_n(y), \qquad G_{mn}^{(b)}(x, y) = -H_m(x)K_n(y),$$
$$G_{mn}^{(c)}(x, y) = -K_m(x)K_n(y), \qquad m = 0, 1; \quad n = 0, 1. \tag{25}$$

Explicit expressions for the integrand functions Γ_{ui} and Γ_{ij} representing the displacement and stress components, respectively, are given in terms of F_{mn} and G_{mn} in the Appendix.

From eqns (22)–(25) and the integrand functions Γ, we observe that while the integrals in the regions (a) and (b) represent complex quantities, the integrands in $1 < q < \infty$ are always real.

The solution to the problem as given by the integral representations of eqns (22) (with the integrands given in the Appendix) is formally complete. Due to the character of the integrands, these integrals are evaluated numerically. (It is observed that possible integration in the complex plane, using residue theory, would lead in any case to a numerical integration of the resulting branch integrals which are due to the multivalued character of the Hankel functions.)

In performing the integrations it is noticed that singularities arise in the given Hankel and Bessel functions at the points $q = 1/\sqrt{3}$ and $q = 1$, as well as in the integrands at points $q = q_R$ which represent roots of $\Lambda(q) = 0$.

At $q = 1/\sqrt{3}$ and $q = 1$ (where $\beta_p \to 0$ and $\beta_s \to 0$, respectively), the Hankel function and modified Bessel functions approach infinity. Upon using series representations as the relevant arguments approach zero, and performing the limiting process on the expressions Γ_{ui}/Λ and Γ_{ij}/Λ in the appropriate regions, the integrands appearing in eqns (22), as defined in eqns (23) and eqns (A1)–(A6), are found to be finite, thus possessing, in effect, removable singularities.

On the other hand, the vanishing of Λ at $q = q_R$ leads to a nonremovable singularity in the integrand at this point. An examination of eqn (23) reveals that the roots $q_R > 1$, i.e. they fall in the region previously denoted as region (c). Written explicitly, the vanishing of $\Lambda^{(c)}$ becomes

$$2\Omega q^2(q^2 - 1)^{1/2}\left(q^2 - \frac{1}{3}\right)^{1/2} K_0(\Omega b_s)K_1(\Omega b_p)$$
$$- \frac{\Omega}{2}(2q^2 - 1)^2 K_1(\Omega b_s)K_0(\Omega b_p) + \left(q^2 - \frac{1}{3}\right)^{1/2} K_1(\Omega b_s)K_1(\Omega b_p) = 0 \tag{26}$$

which, with appropriate changes of notation, is recognized as the same equation obtained by Biot[14] in his study of waves propagating along a bore. The contributions arising from these singularities represent surface waves (similar to Rayleigh waves), and are discussed in the next section.

No particular difficulty results due to this singularity, since it arises due to a simple zero of Λ. As the remaining parts of the integrands are well behaved in the neighborhood of $q = q_R$, the integrals of region (c) are evaluated in the sense of Cauchy's Principal value, i.e.

$$\text{P.V.} \int_1^\infty f(q)\, dq = \lim_{\epsilon \to 0} \left(\int_1^{q_R - \epsilon} f(q)\, dq + \int_{q_R + \epsilon}^\infty f(q)\, dq \right). \tag{27}$$

Finally, convergence of the integrals as $q \to \infty$, and the numerical integration of the indefinite integral over the infinite range must be treated. For $q \gg 1$ and $q \gg \Omega$, the integrals are evaluated asymptotically following a procedure used in a previous investigation[7]. Asymptotic results using this procedure are again given in [11].

4. INTERPRETATION OF ANALYTICAL EXPRESSIONS AND NUMERICAL RESULTS

(a) *Interpretation of analytical expressions*

In anticipation of the numerical results presented below, it is worthwhile to examine first the general integral expressions for the displacement and stress components given by eqns (22) and (23), together with the integrands given by eqns (A1)–(A6). From these equations we note that the desired quantities, in general, are expressed in terms of three integrals. Moreover, from the definition of the integrand functions, the integrals are seen to have the following dependencies in the three regions a, b and c:

$$I_a \to H_n^{(1)}(\beta_s\rho),\ H_n^{(1)}(\beta_p\rho),$$

$$I_b \to H_n^{(1)}(\beta_s\rho),\ K_n(\beta_p\rho),$$

$$I_c \to K_n(\beta_s\rho),\ K_n(\beta_p\rho).$$

Recalling that the H_n functions represent sinusoidal functions decaying as $\rho^{-1/2}$, and that the K_n functions decay monotonically, we conclude, upon examining the product of these functions with $\exp(-i\Omega\tau)$, that the complex I_a integrals represent radiating P- and S-waves; the complex I_b integrals represent radiating S-waves only, and that the real I_c integrals contribute no radiating P- or S-waves. This character of the solution and corresponding contributions to the response are represented schematically in Fig. 2.

It is of importance to consider also the propagation of waves in the z-directions with phase velocity C. We first note that the terms $(\cos\alpha\xi)\,e^{-i\Omega\tau}$ or $(\sin\alpha\xi)\,e^{-i\Omega\tau}$ represent the propagation of waves of wavelength

$$\lambda = 2\pi a/\alpha, \tag{28}$$

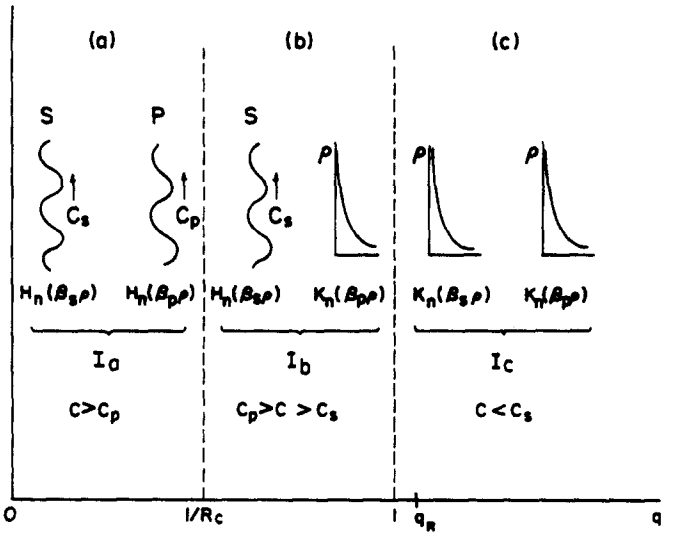

Fig. 2. Response contributions.

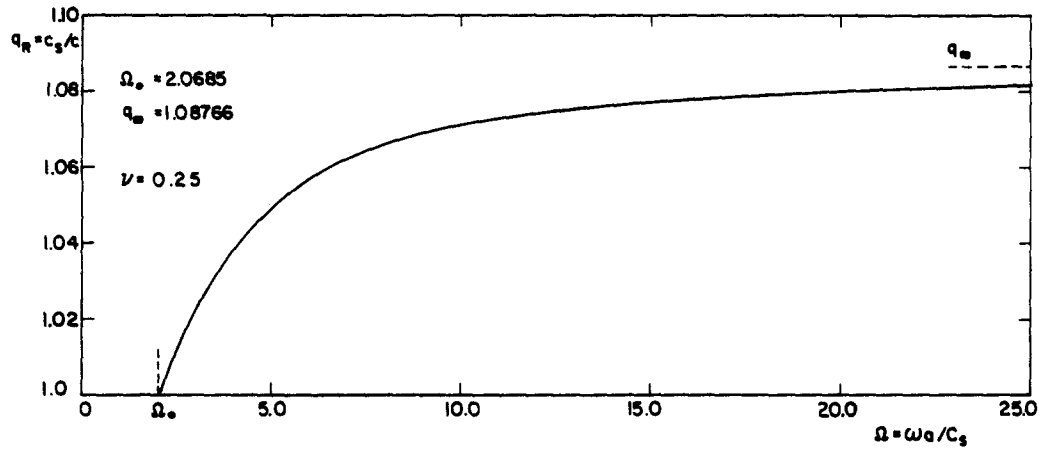

Fig. 3. Dispersion curve of surface waves.

which propagate with respect to the z-direction with a phase velocity $C = f\lambda$, where f is the forcing frequency of the steady-state solution. The integral representation may then be considered as the sum of wave contributions of varying wavelength from $\lambda \to \infty$ ($\alpha = 0$) to $\lambda = 0$ ($\alpha \to \infty$). From the definitions $\Omega = \omega a/C_s$ and $R_c = C_p/C_s$ (here $R_c = \sqrt{3}$), and taking into account the definitions given in eqns (20) and (21), we conclude that, in effect, $q = C_s/C$. Hence, the P-waves propagate with a phase speed $C > C_p$, and S-waves propagate with phase speed $C > C_s$. Waves with wavelength $\lambda < 2\pi a/\Omega$ thus cannot propagate as P- or S-waves; this is revealed by the representation of the I_c integrals which consist of radially decaying distribution patterns.

The behavior resulting from the singularity of the integrands arising at the point $q = q_R > 1$ [given by the real roots of eqn (26)], remains to be considered. As was previously noted, the singularities of these integrands correspond to surface waves which propagate along the bore surface. The root $q_R > 1$ corresponds, therefore, to a wave propagating with phase velocity $C < C_s$. The real roots q_R of eqn (26) were obtained numerically for parametric values of Ω, and are presented in Fig. 3. Thus, since $q_R = q_R(\Omega)$, the resulting surface waves are dispersive in contradistinction to nondispersive Rayleigh waves on a plane surface. We observe that the roots fall in the range $1 < q_R < 1.08766$. The upper bound (which corresponds also to $a \to \infty$), in fact, represents the propagation of Rayleigh surface waves with $\nu = 0.25$. We observe, too, that there exists a cutoff frequency $\Omega = \Omega_0 = 2.0685$ given by the root of the equation

$$2\sqrt{(2/3)}\, K_1(\Omega\sqrt{2/3}) = \Omega\, K_0(\Omega\sqrt{2/3}), \tag{29}$$

which represents the limiting equation of eqn (26) with $q = 1$. This result agrees with the fact that the surface phase-speed C can never be greater than C_s. A physical interpretation of this result is given, e.g. in [15]. (This cutoff was obtained in different form by Biot[14]).

Thus for all frequencies $0 < \Omega < \Omega_0$, no singularities will exist in the integrals I_c. Physically, this signifies that for forcing frequencies in this range, no surface waves will be excited. Conversely, for any given forcing frequency $\Omega > \Omega_0$, a surface wave, of length $\lambda = 2\pi a/q_R\Omega$, will be excited and will propagate with phase speed $C = C_s/q_R$. Such a wave, corresponding to free propagating surface waves, contributes a resonance-type effect which is reflected by the singular behavior of the integrands at $q = q_R$. Naturally, given the continuous spectrum of wave summations, true resonance does not take place.

(b) *Numerical results*

Results of particular interest are those which measure the penetration of the response into the medium. Consequently, curves are presented for the nonvanishing

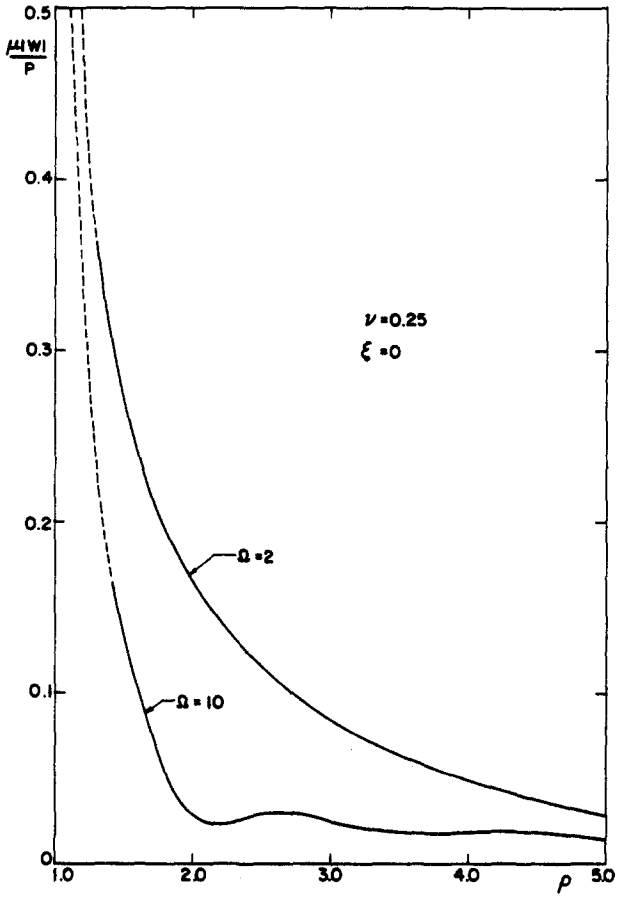

Fig. 4. Radial displacement along line $\xi = 0$.

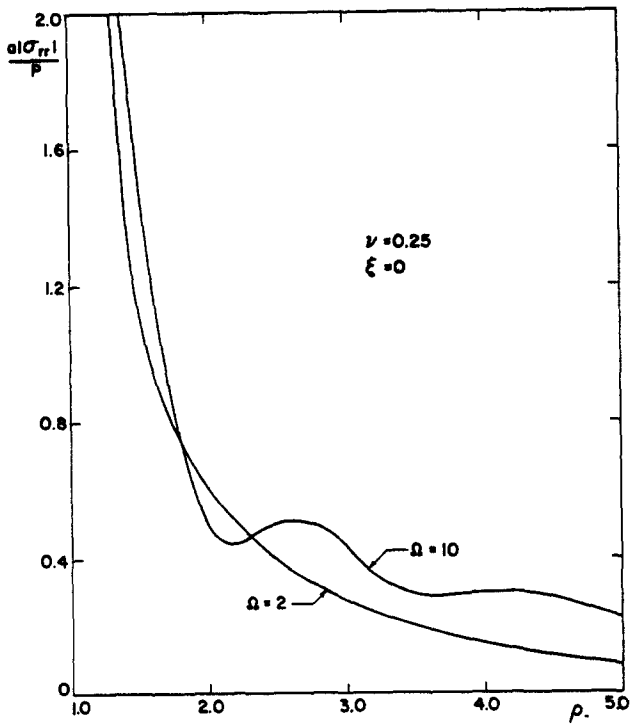

Fig. 5. Stress σ_{rr} along line $\xi = 0$.

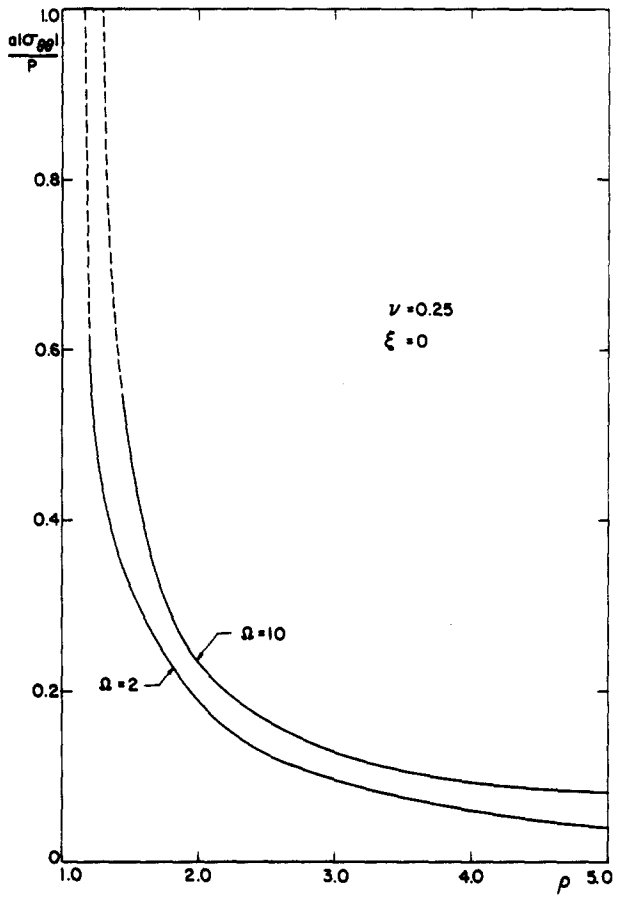

Fig. 6. Stress $\sigma_{\theta\theta}$ along line $\xi = 0$.

displacement and stress components along the radial line, $\xi = 0$, emanating from the point of load application.

Since the total response is composed, as discussed above, in terms of complex quantities, significant results for the steady-state response are given in terms of the amplitudes of displacements and stresses, $\mu \mid u_i \mid /P$, $a \mid \sigma_{ij} \mid /P$. Numerical results for the radial displacement amplitude $\mid w \mid$ and nonvanishing stress components $\mid \sigma_{rr} \mid$, $\mid \sigma_{\theta\theta} \mid$ and $\mid \sigma_{zz} \mid$ along the radial line are presented in Figs. 4–7 as a function of the radial distance ρ for a relatively low value of Ω, $\Omega = 2$, and for a large value, $\Omega = 10$. The displacement and stresses are observed to be very large in the neighborhood of the applied load and to decay rapidly with increasing ρ.† For the low-frequency case, $\Omega = 2.0$, the decay is seen in all figures to be monotonic (and similar to the static response given in [3]), while for the high-frequency case, the curves show, in general, an oscillating decay. It is observed that $\mid w \mid$ is larger for the smaller value of Ω, while the opposite is true for the stress components; i.e. higher frequencies tend to produce higher stresses. (A similar pattern of behavior was noted for the simpler case of torsional loads given in [7].)

Of particular interest is a comparison of the dynamic behavior with the corresponding static behavior given in [3]; this is most effectively represented by means of the ratio of dynamic response to static response, viz. the dynamic amplification factors $\mid w_D/w_S \mid$ and $\mid \sigma_{ij,D}/\sigma_{ij,S} \mid$. These ratios are presented in Figs. 8–11.

† The results presented, obtained using a numerical integration procedure, are valid in general to three places for $\rho > 1.2$. In the region of the applied load, as $\rho \to 1$, singularities arise due to the slow convergence of the integrals with large values of q. Such singularities have been previously found, and their strengths determined in the corresponding static case[16]. Results as $\rho \to 1$, appearing in Figs. 4–7, could only be evaluated to lesser accuracy, and are therefore shown as broken lines. Details of the numerical computations are given in [11].

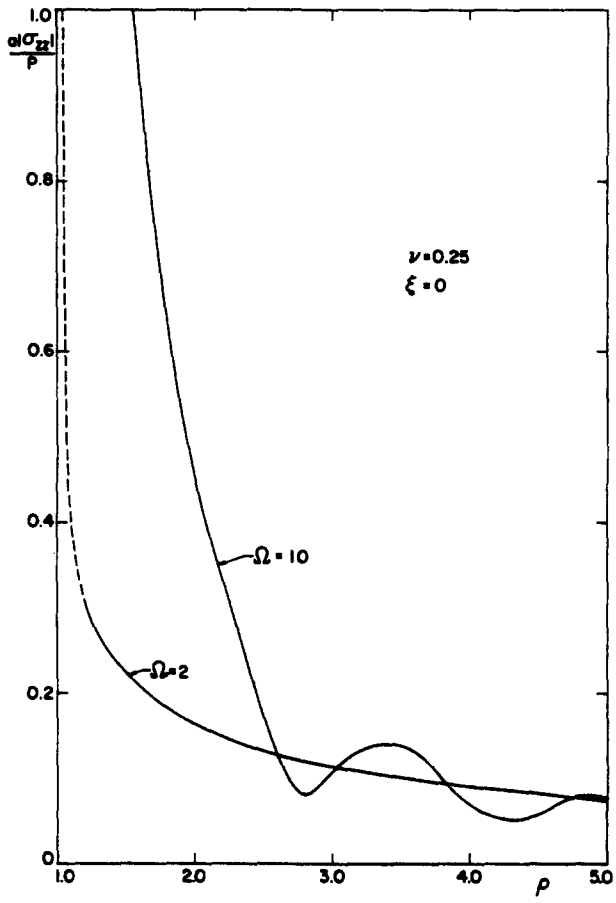

Fig. 7. Stress σ_{zz} along line $\xi = 0$.

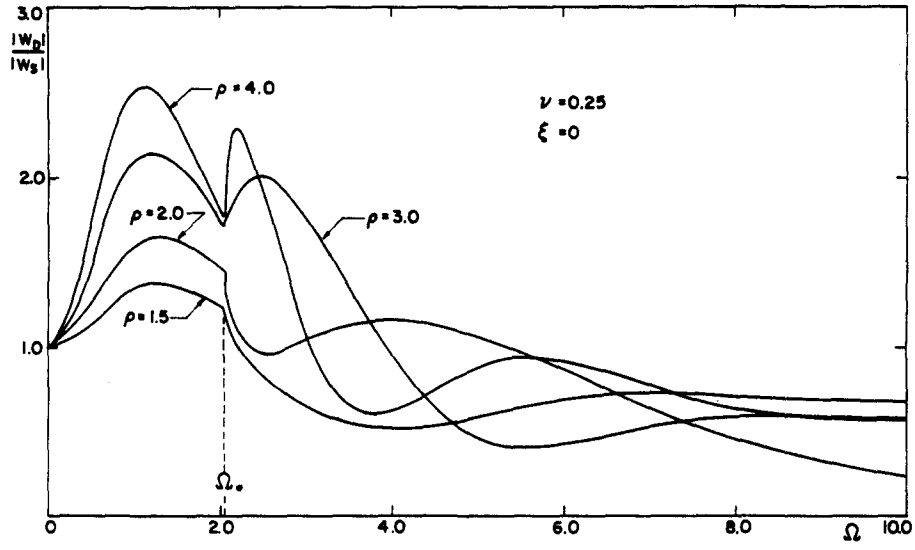

Fig. 8. Dynamic amplification factor for w.

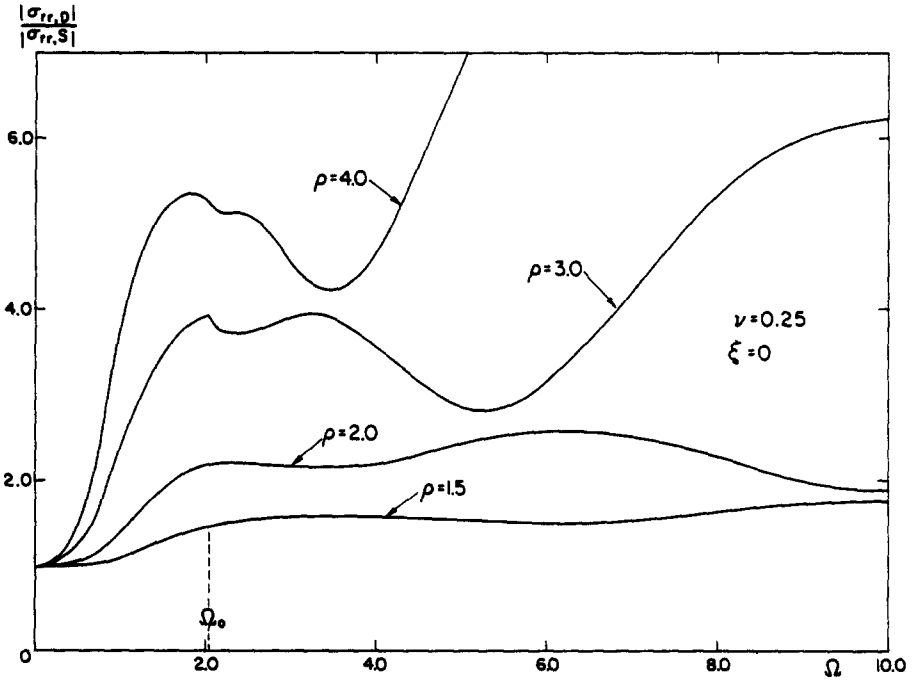

Fig. 9. Dynamic amplification factor for σ_{rr}.

In Fig. 8, $| w_D/w_s |$ is shown as a function of the nondimensional frequency Ω for four values of ρ: $\rho = 1.5, 2.0, 3.0$ and 4.0. It is observed that the ratios start at $\Omega = 0$ from unity,‡ reach a peak in the vicinity of $\Omega \approx 1$ and decay smoothly for all values of $\Omega < \Omega_0$. At the point $\Omega = \Omega_0$ the response changes behavior, as reflected either by a cusp in the curve (for lower values of ρ), or by a new peak (for points farther away

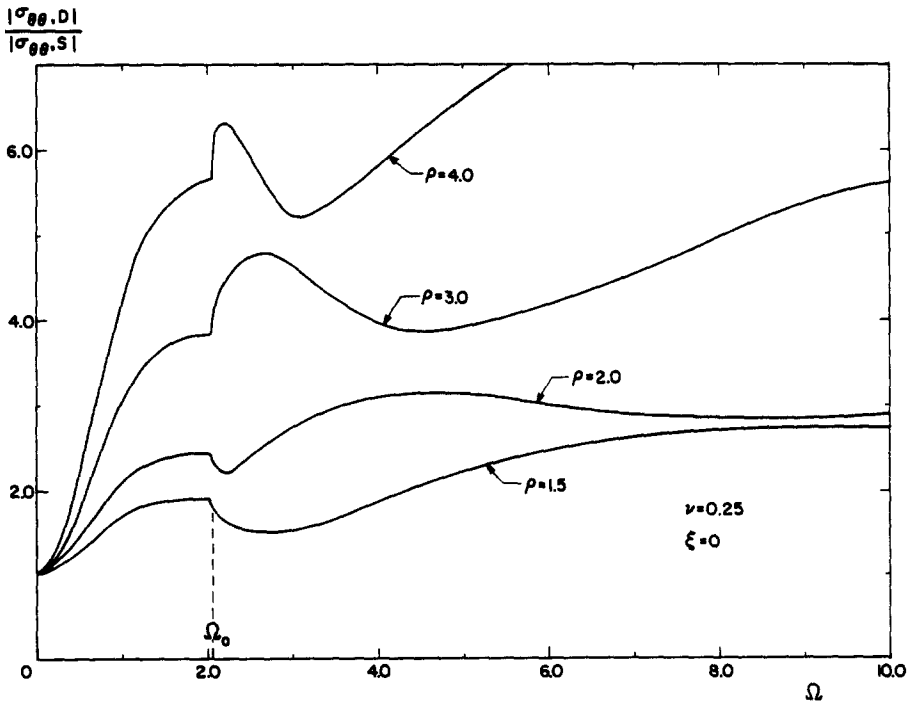

Fig. 10. Dynamic amplification factor for $\sigma_{\theta\theta}$.

‡ In a sense, this result provided a numerical check on the dynamic calculations, since the static response taken from [3] was based on independent calculations and algorithms.

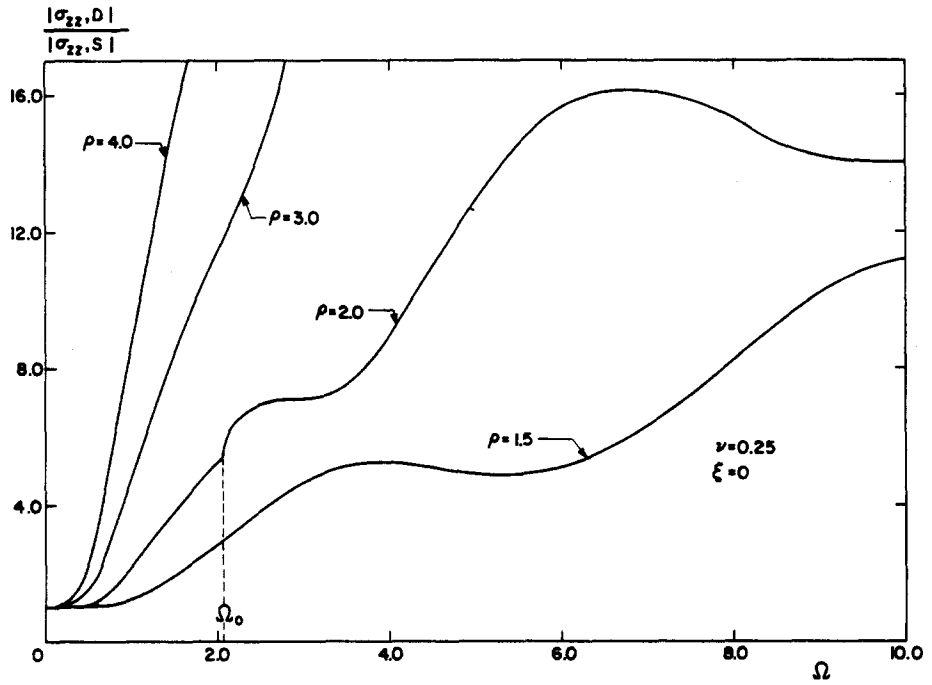

Fig. 11. Dynamic amplification factor for σ_{zz}.

from the bore surface). This abrupt change in response patterns at $\Omega = \Omega_0$ is clearly due to the sudden excitation of surface waves, as discussed previously. For increasing values of Ω, the displacement dynamic amplification factor is observed, for all field points ρ, to exhibit an oscillatory decay to values less than unity. It should be noted, however, that in general the amplification factors still increase with larger values of ρ.

The stress amplification factors $|\sigma_{ij,D}/\sigma_{ij,s}|$ are similarly presented in Figs. 9–11 as a function of Ω. Here the curves all increase monotonically with Ω up to $\Omega = \Omega_0$. At this value, an abrupt change in behavior again occurs due to the introduction of the surface wave response. As opposed to the displacement curves, which tend to decay with increasing Ω, thereby showing a dynamic attenuation effect for large Ω, the stress curves show an amplification effect.

The essential feature of the stress-amplification curves is the increasingly greater amplification for increasing values of ρ. This feature is reflected in all the stress curves.

5. DISCUSSION AND CONCLUSIONS

From the results presented, we observe that the spatial distribution of the displacement and stress components, due to the application of time-harmonic pressures with low frequencies, approach those existing in the corresponding static case, while for higher forcing frequencies, nonmonotonically decaying distributions occur. In all cases, however, curves for the dynamic amplification factors, as expected, approach unity for $\Omega \to 0$.

For all governing parameters, the dynamic effect, both for displacement and stresses, becomes stronger with larger values of ρ. Thus the dynamic effect causes the radial penetration of the response to increase significantly. The interpretation of the analytic expressions given in the previous section leads readily to an explanation of this phenomenon. For relatively large values of ρ, the static solution is increasingly small, as reflected by an exponentially decaying pattern. On the other hand, the dynamic response consists of radiating P- and S-waves, which decay as $\rho^{-1/2}$. The ratio of the dynamic to static response will therefore necessarily increase with ρ; hence, far greater radial penetration due to the dynamic effect.

The variation of the response with forcing frequency shows that for increasingly

higher frequencies, the displacement at a given field point becomes increasingly attenuated, while the stress response is amplified.

Practical implications of these results lead to the conclusion that in order to increase the region of high-stress values, it is preferable to apply pressures to the bore surface with increasing high frequencies. Within such regions it should be possible, using appropriate failure criteria, to delineate effective zones of crack formation in the medium.

REFERENCES

1. C. J. Tranter, On the elastic distortion of a cylindrical hole by a localized hydrostatic pressure. *Q. Appl. Math.* **4**, 298–302 (1946).
2. O. L. Bowie, Elastic stresses due to a semi-infinite band of hydrostatic pressure acting over a cylindrical hole in an infinite solid. *Q. Appl. Math.* **5**, 100–101 (1947).
3. R. Parnes, Applied tractions on the surface of an infinite cylindrical bore. *Int. J. Solids Structures* **19**, 165–177 (1983).
4. W. L. Selberg, Transient compression waves from spherical and cylindrical cavities. *Ark. Fys.* **5**, 97–108 (1952).
5. D. W. Jordan, The stress wave from a finite cylindrical explosive source. *J. Math. Mech.* **11**(4), 503–551 (1962).
6. S. K. Datta, A. H. Shah and N. El-Akily, Dynamic behavior of a buried pipe in a seismic environment. *J. Appl. Mech.* **49**(1), 141–148 (1982).
7. R. Parnes, Elastic response to a time-harmonic torsion-force acting on a bore surface. *Int. J. Solids Structures* **19**(10), 925–934 (1983).
8. M. K. Hubbert and D. G. Willis, Mechanics of hydraulic fracturing. *AIME Petrol. Trans.* **210**, 153–166 (1957).
9. A. A. Danesby, On the design of vertical hydraulic fractures. *J. Petrol. Tech.* **25**, 83–93 (1973).
10. R. Parnes, Response of an infinite elastic medium to traveling loads in a cylindrical bore. *J. Appl. Mech.* **36**(1), 51–58 (1969).
11. R. Parnes, Steady-state concentrated pressure loading on a bore hole surface. Tel-Aviv University, Report No. SOE-1-83 (1983).
12. I. N. Sneddon, *Fourier Transforms*, McGraw-Hill, New York (1951).
13. N. W. McLachlan, *Bessel Functions for Engineers*, Oxford University Press, Oxford (1955).
14. M. A. Biot, Propagation of elastic waves in a cylindrical bore containing a fluid. *J. Appl. Phys.* **23**(9), 997–1005 (1952).
15. R. Parnes, Dispersion relations of a rod embedded in an elastic medium. *J. Sound Vib.* **76**(1), 65–75 (1981).
16. R. Parnes, On singularities due to a concentrated pressure loading of a cylindrical cavity, *Int. J. Solids Structures* **20**, 267–276 (1984).

APPENDIX: EXPRESSIONS FOR INTEGRANDS Γ APPEARING IN INTEGRAL REPRESENTATIONS OF DISPLACEMENT AND STRESS COMPONENTS, EQN (22)

Integral representations for the nonvanishing displacement and stress components are given below for each region: (a) $0 < q < 1/\sqrt{3}$; (b) $1/\sqrt{3} < q < 1$ and (c) $1 < q < \infty$.

Using the definitions of eqns (19)–(21), (24) and (25), the integrand functions Γ_{u_i} and Γ_{ij} for the displacement and stress components, respectively, are given as follows in each of the above regions, k = a, b or c:

$$\Gamma_w^{(k)} = b_p \left[\frac{1}{2}(2q^2 - 1)F_{11}^{(k)}(\beta_s, \beta_p\rho) - q^2 F_{11}^{(k)}(\beta_s\rho, \beta_p)\right] \cos(\Omega\xi q), \tag{A1}$$

$$\Gamma_u^{(k)} = q\left[\frac{1}{2}(2q^2 - 1)F_{10}^{(k)}(\beta_s, \beta_p\rho) + b_s b_p G_{01}^{(k)}(\beta_s\rho, \beta_p)\right] \sin(\Omega\xi q), \tag{A2}$$

$$\Gamma_{rr}^{(k)} = \left\{-(2q^2 - 1)\left[\frac{1}{2}(2q^2 - 1)\Omega F_{10}^{(k)}(\beta_s, \beta_p\rho) + \frac{b_p}{\rho} F_{11}^{(k)}(\beta_s, \beta_p\rho)\right] + 2q^2 b_p\left[\frac{1}{\rho} F_{11}^{(k)}(\beta_s\rho, \beta_p) - \Omega b_s G_{01}^{(k)}(\beta_s\rho, \beta_p)\right]\right\} \cos(\Omega\xi q), \tag{A3}$$

$$\Gamma_{\theta\theta}^{(k)} = \left\{(2q^2 - 1)\left[\frac{\Omega}{6} F_{10}^{(k)}(\beta_s, \beta_p\rho) + \frac{b_p}{\rho} F_{11}^{(k)}(\beta_s, \beta_p\rho)\right] - \frac{2q^2 b_p}{\rho} F_{11}^{(k)}(\beta_s\rho, \beta_p)\right\} \cos(\Omega\xi q), \tag{A4}$$

$$\Gamma_{zz}^{(k)} = \Omega\left[\frac{1}{2}(1/3 + 2q^2)(2q^2 - 1)F_{10}^{(k)}(\beta_s, \beta_p\rho) + 2q^2 b_s b_p G_{01}^{(k)}(\beta_s\rho, \beta_p)\right] \cos(\Omega\xi q), \tag{A5}$$

$$\Gamma_{rz}^{(k)} = \Omega b_p q(2q^2 - 1)\left[F_{11}^{(k)}(\beta_s\rho, \beta_p) - F_{11}^{(k)}(\beta_s, \beta_p\rho)\right] \sin(\Omega\xi q). \tag{A6}$$